Cloud-Radiative Forcing and Climate: Results from the Earth Radiation Budget Experiment

V. RAMANATHAN, R. D. CESS, E. F. HARRISON, P. MINNIS, B. R. BARKSTROM, E. AHMAD, D. HARTMANN

The study of climate and climate change is hindered by a lack of information on the effect of clouds on the radiation balance of the earth, referred to as the cloud-radiative forcing. Quantitative estimates of the global distributions of cloud-radiative forcing have been obtained from the spaceborne Earth Radiation Budget Experiment (ERBE) launched in 1984. For the April 1985 period, the global shortwave cloud forcing [−44.5 watts per square meter (W/m^2)] due to the enhancement of planetary albedo, exceeded in magnitude the longwave cloud forcing (31.3 W/m^2) resulting from the greenhouse effect of clouds. Thus, clouds had a net cooling effect on the earth. This cooling effect is large over the mid- and high-latitude oceans, with values reaching −100 W/m^2. The monthly averaged longwave cloud forcing reached maximum values of 50 to 100 W/m^2 over the convectively disturbed regions of the tropics. However, this heating effect is nearly canceled by a correspondingly large negative shortwave cloud forcing, which indicates the delicately balanced state of the tropics. The size of the observed net cloud forcing is about four times as large as the expected value of radiative forcing from a doubling of CO_2. The shortwave and longwave components of cloud forcing are about ten times as large as those for a CO_2 doubling. Hence, small changes in the cloud-radiative forcing fields can play a significant role as a climate feedback mechanism. For example, during past glaciations a migration toward the equator of the field of strong, negative cloud-radiative forcing, in response to a similar migration of cooler waters, could have significantly amplified oceanic cooling and continental glaciation.

CLOUDS ARE REGULATORS OF THE RADIATIVE HEATING OF the planet. They reflect a large part of the incoming solar radiation, causing the albedo of the entire earth to be about twice what it would be in the absence of clouds (*1*). Clouds also absorb the longwave (LW) radiation (also known as infrared or thermal radiation) emitted by the warmer earth and emit energy to space at the colder temperatures of the cloud tops. Cloud LW absorption and emission are, in a sense, similar to the radiative effects of atmospheric gases. The combined effect of LW absorption and emission—that is, the greenhouse effect—is a reduction in the LW radiation emitted to space. The greenhouse effect of clouds may be larger than that resulting from a hundredfold increase in the CO_2 concentration of the atmosphere (*2*).

How these two competing effects of clouds vary with time, geography, or cloud type and structure is not well understood; nor do we know how clouds modulate meridional and regional radiative heating. Such heating drives the general circulation of the atmosphere and oceans. Significantly different estimates of cloud radiative effects have been used in models of past and future climates. In short, the fundamental question, whether clouds cool or warm the climate, has remained unanswered.

Cloud-radiative interactions represent a large source of uncertainty in several areas including: (i) the prediction of climate changes associated with an anthropogenic increase in trace gases, and (ii) the understanding of past and future climate changes caused by variations in the solar constant or the orbital parameters of the earth (*3, 4*). General circulation model (GCM) studies (*4*) have contributed to our understanding of cloud-climate feedback, and limited observational studies (*5*) have aided the identification of complex mechanisms of cloud-climate interaction. However, a global perspective on cloud-radiative interactions based on observations has been lacking.

Observations of the modulation of the solar and LW radiation fluxes by clouds can provide needed insights into the cloud-climate interaction. Such modulations are called the shortwave (SW) and longwave cloud-radiative forcing (*6*). We have obtained quantitative estimates of the global distributions of SW and LW forcing from the Earth Radiation Budget Experiment (ERBE), a system of satellites that provides data on incoming and emitted radiation (*7*). In this article, we develop the cloud-radiative forcing concept, describe global variations in the forcing on the basis of the ERBE data, and, finally, discuss the implications of these data for understanding past and future climatic changes.

Description of ERBE. The ERBE includes three satellites in different orbits, a system that improves temporal sampling and can provide data on diurnal variations. The Space Shuttle Challenger launched the first of three satellites, the Earth Radiation Budget Satellite (ERBS), in October 1984. The second satellite (National Oceans and Atmospheric Agency, NOAA-9) was launched in December 1984. The third (NOAA-10) was launched in July 1986 (*8*). In our study, we used data gathered by the ERBS and NOAA-9 satellites. Each satellite contained a pair of instrument packages: a scanner and a nonscanner; we used the scanner measurements only. The scanner footprint at nadir, that is, looking down, was about 35

V. Ramanathan is a professor in the Department of Geophysical Sciences, University of Chicago, Chicago, IL 60637. R. D. Cess is a professor at the Institute for Atmospheric Sciences, State University of New York at Stony Brook, Stony Brook, NY 11794. E. F. Harrison, P. Minnis, and B. R. Barkstrom are with the Atmospheric Sciences Division, NASA Langley Research Center, Hampton, VA 23665. E. Ahmad is in the Department of Geophysical Sciences, University of Chicago, Chicago, IL 60637. D. Hartmann is a professor in the Department of Atmospheric Sciences, University of Washington, Seattle, WA 98195.

km. During flight, observations of internal black bodies and the sun were used to calibrate the measurements. Independently monitored tungsten lamps also provided a relative check of the SW calibration. A solar monitor on the nonscanner instrument measures solar irradiance. We use this measurement to calculate the geographic distribution of incident sunlight. The instruments on the scanner measure the reflected SW and the emitted LW fluxes at the top of the atmosphere. The difference between the incident flux and the reflected SW flux gives the solar energy absorbed by the surface-atmosphere column. The emitted LW flux is the energy radiated away by the column. The difference between the absorbed and emitted flux is the net radiative heating of the surface-atmosphere column. We combined the radiation budget data from ERBS and NOAA-9 satellites to produce diurnal average fluxes on a daily basis. Then, we averaged these daily fluxes over the days in the month to produce the data presented. We discuss below the completed analyses for April 1985. Our initial analyses of data available for other months support the conclusions based on the April 1985 data.

The cloud-radiative forcing concept. Let us consider a domain of an area large enough to contain regions of overcast skies and regions of clear skies. In the overcast regions, water vapor occurs with condensed water or ice, or both; in the clear sky regions, water occurs only in the vapor phase. The domain can be the whole earth, an entire latitude belt, or a specific region on the globe. Typically, such a domain would be a composite of overcast and clear skies and is referred to, usually, by meteorologists as cloudy. The term cloudy should not be confused with the term overcast. A cloudy domain is overcast only when it is completely covered with clouds.

The net radiative heating, H, for the entire surface-to-atmosphere column of a cloudy domain is

$$H = S(1 - \alpha) - F \quad (1)$$

where S is the solar irradiance and α is the albedo; hence $S(1 - \alpha)$ is the absorbed solar radiation. F is the LW flux emitted to space.

To describe the effects of clouds on H from observations, we first define the cloud forcing C

$$C = H - H_{clr} \quad (2)$$

where H_{clr} is the clear-sky net heating. If a domain has no clouds, $H = H_{clr}$ and $C = 0$. Thus, clouds should cause any difference between the net radiative heating averaged over the domain and the

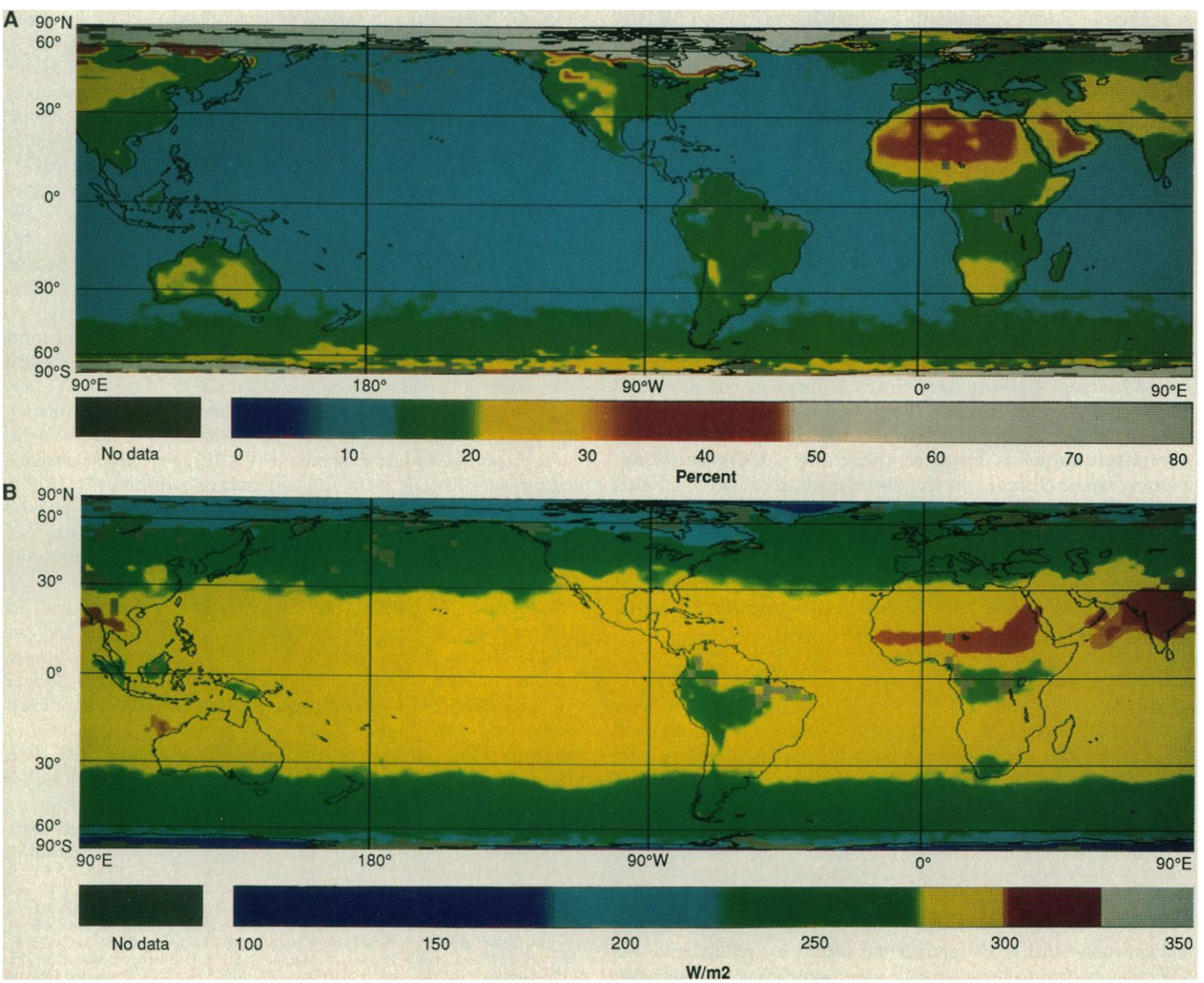

Fig. 1. (**A**) Clear-sky albedo; monthly averages for April 1985. Data from the scanners on-board ERBS and NOAA-9 satellites have been combined; (**B**) same as (A), but for clear-sky LW flux.

heating averaged only over the clear-sky regions in that domain. From Eqs. 1 and 2, we can write C as

$$C = C_{SW} + C_{LW} \quad (3)$$

where $C_{SW} = S(\alpha_{clr} - \alpha)$ and $C_{LW} = F_{clr} - F$; α_{clr} is the clear-sky albedo and F_{clr} is the clear-sky LW radiation flux.

Clouds are almost always more reflective than the ocean surface and land, except where there is snow. Thus, when clouds are present, they reflect more solar energy into space than would clear skies. The SW cloud forcing, C_{SW}, gives a quantitative estimate of this effect. C_{SW} is simply the difference between the clear-sky and cloudy-sky reflected solar fluxes. When clouds are present, the atmospheric column radiates less thermal energy into space than it would if the skies were clear. The LW cloud forcing (C_{LW}) measures this effect. The net effect of clouds is simply the sum of the LW and SW cloud forcing (Eq. 3). Equations 1 to 3 can also be derived in a slightly different way (*6*), which leads to a cloud forcing expression in cloud fraction and radiative fluxes from overcast skies. For example, $C_{SW} = S(\alpha_{clr} - \alpha)$ is equal to

$$S(\alpha_{clr} - \alpha) = S \sum_i f_i (\alpha_{clr,i} - \alpha_{o,i}) \quad (4)$$

In Eq. 4, the domain is subdivided into i subregions; f_i is the cloud fraction and $\alpha_{o,i}$ is the overcast albedo for region i.

Obtaining the forcing from the expression on the left-hand side of Eq. 4 is simpler and more effective than obtaining it from the right-hand side. First, the clear-sky fluxes are significantly more homogeneous than overcast sky fluxes. As a result, the extension of clear-sky fluxes to the entire domain minimizes the errors caused by poor spatial and temporal sampling. Second, estimation of poorly constrained quantities, such as cloud fractions, is not necessary. Thus, obtaining the cloud-radiative forcing reduces to the relatively simple (but still difficult) problem of measuring the clear-sky fluxes (*9*).

The spatial resolution of meteorological scanners is not small enough to allow identification of all the clear-sky areas in a region, but this is not a problem because we do not anticipate systematic variations in the clear-sky fluxes as a function of resolution. Clear scenes that are larger than the resolution of the telescope should have the same fluxes as smaller clear scenes. Observations for periods longer than a week should average variations caused by random scene-to-scene differences. Another potential problem occurs where an entire region is overcast. In such regions, we can still infer a cloud forcing by enlarging the size of the region so that it includes some clear skies. An equivalent procedure is the adoption of an average of the clear-sky fluxes estimated for the surrounding regions. The uncertainty in the estimates increases with the spatial inhomogeneity of regional-scale clear-sky fluxes. Our results show that the clear-sky fluxes among adjacent regions are significantly more homogeneous than the fluxes for average cloudy conditions.

ERBE observations of clear-sky albedo and LW flux. The distribution of clear-sky albedo (Fig. 1A) reveals that the oceans are the darkest regions of the globe. They have albedos that range from 6 to 10 percent in the low latitudes to 15 to 20 percent near the poles. Ocean albedo increases toward high latitudes because the albedo of the surface increases as the sun lowers in the sky (*10*). The brightest parts of the globe are the snow-covered Arctic and Antarctic. Next in brightness to the snow-covered regions are the major deserts. The Saharan and Saudi Arabian deserts reflect as much as 40 percent of the incident solar radiation. The other major deserts, the Gobi and Gibson deserts, reflect about 25 to 35 percent. The tropical rain forests in South America and Central Africa have albedos from 10 to 15 percent. They are the darkest land surfaces on the earth.

The clear-sky LW radiation data (Fig. 1B) show a more systematic pattern. Emission decreases from a maximum of 330 W/m^2 in the tropics to about 150 W/m^2 in the polar regions. Although the clear-sky observations contain no major surprises, they do provide quantitative estimates of the distribution of clear-sky radiative heating.

Statistics of clear-sky fluxes and uncertainties. The accuracy of the estimates for regional and time-averaged clear-sky fluxes depends on the homogeneity of the clear region fluxes. The spatial resolution of the scanner is not sufficient to detect all of the clear regions in the domain of interest. The error attributed to this poor sampling depends on the spatial and temporal variability of the clear-sky fluxes. To demonstrate that the clear-sky flux estimates were accurate, we computed their standard deviation (σ) for several spatial

Table 1. Standard deviation of clear-sky LW and SW fluxes (in parentheses) in watts per meter squared. Four overlapping scans were used to estimate the pixel scale σ's. Each scan contains 62 pixels. All of the clear-sky pixels in the four-scan set entered the computation of a mean and a standard deviation. The pixels were also sorted into 2.5° by 2.5° regions. The clear-sky data for 1 day then yield regional σ values. The 1-day σ's for each 2.5° latitude belt were averaged. For the daily average, the σ of 30 daily mean values was computed for each region and the σ's were averaged over a latitude belt.

Latitude zone	Pixel scale	Regional scale	Daily (regional scale)
42.5°N to 47.5°N	3.9 (8.3)	7.7 (3.1)	4.3 (3.5)
27.5°N to 32.5°N	2.7 (8.9)	4.1 (2.0)	6.5 (4.2)
2.5°N to 2.5°S	3.2 (6.3)	2.5 (1.8)	3.9 (3.2)
27.5°S to 32.5°S	4.0 (9.3)	2.4 (1.5)	5.5 (5.5)
42.5°N to 47.5°S	1.8 (4.5)	3.9 (2.0)	5.4 (4.6)

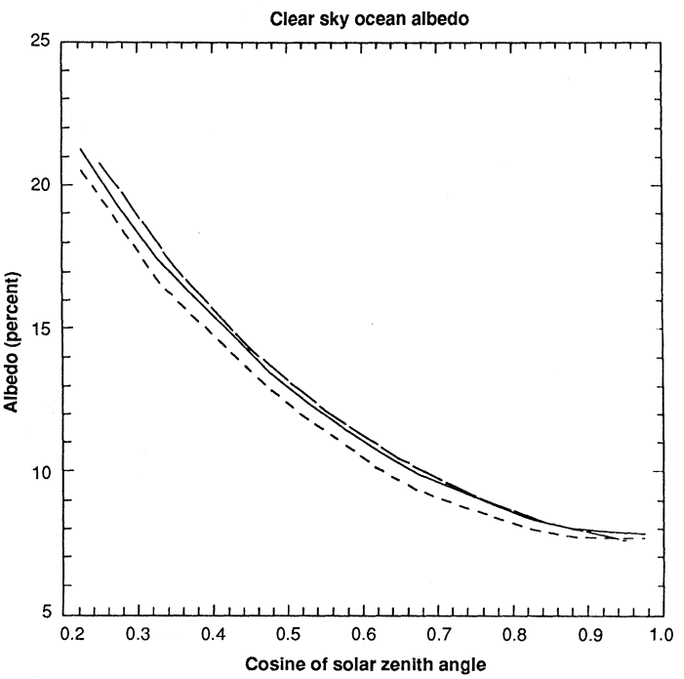

Fig. 2. Clear-sky ocean albedos. (solid line) Observed albedos for April 1985. The albedos were inferred from the scanner pixel data with the use of the operational ERBE algorithm for identifying clear-sky scenes. A total of 1,280,047 scanner pixels covering the global oceans was included. (Short dash) Same as the solid curve but, in addition to the operational algorithm, a stringent homogeneity criterion was used; a total of 50,640 pixels was included. (Long dash) Computed albedos from the model described in (*10*). In this model, observed ocean surface reflectivities are used in a multiple-scattering model that accounts for Rayleigh and aerosol scattering and absorption by O_3, H_2O, and CO_2.

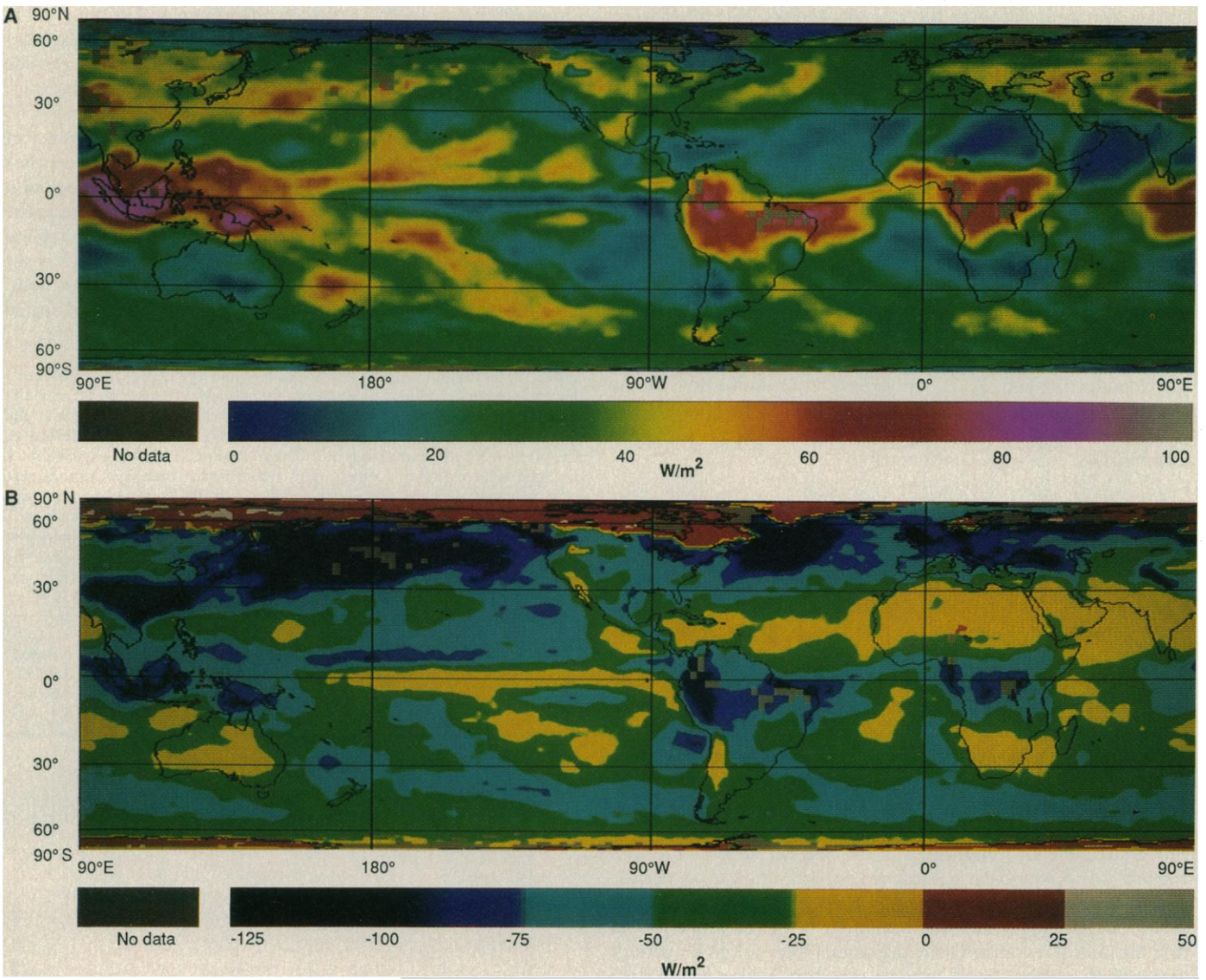

Fig. 3. The LW (**A**) and SW (**B**) cloud forcing for April 1985. The uncertainties in the estimated values are about ±10 W/m². Estimates over snow-covered regions may potentially have larger uncertainties because of difficulty in distinguishing clear from cloudy regions over the bright snow-covered regions.

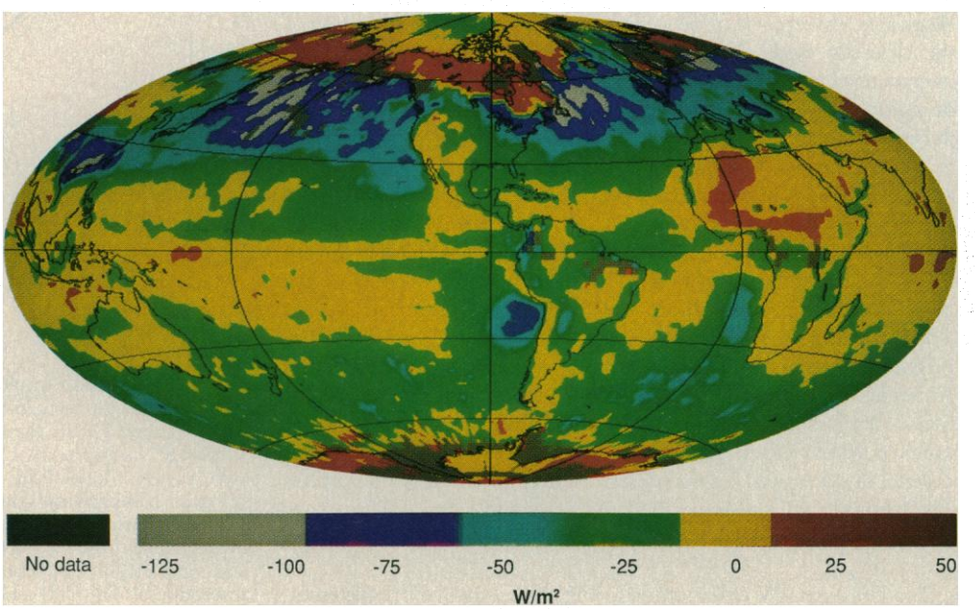

Fig. 4. Net (C_{LW} + C_{SW}) cloud forcing for April 1985. The positive values of cloud forcing, including those seen in North America and in the polar regions, do not exceed 25 W/m².

Table 2. Global summary of radiation budget. Average incident solar radiation for April was 342 W/m^2.

Item	Albedo (%)	SW absorbed (W/m^2)	LW emitted (W/m^2)	NET heating (W/m^2)
Clear sky	16.5	285.6	265.8	19.8
Average	29.5	241.1	234.5	6.6

Table 3. Comparison of global cloud forcing estimates in watts per meter squared.

	ERBE data (W/m^2)				GCM's†
	April 1985	July 1985*	October 1985*	January 1986*	
C_{LW}	31.3	30	32	30.6	23 to 55
C_{SW}	−44.5	−46.4	−49.4	−51.9	−45 to −74
C	−13.2	−16.4	−17.4	−21.3	+1 to −34

*Analysis not completed for these months. †On the basis of a summary of six model studies (*16*) for model simulations with January and July boundary conditions.

and temporal scales (Table 1). The clear-sky σ's were always less than 10 W/m^2 (Table 1). In addition, sampling error for the monthly averaged regional estimates would be even smaller than the σ's shown in Table 1 (*11*). Thus, the statistics in Table 1 suggest that sampling errors for regional clear-sky fluxes are significantly smaller than the regional cloud forcing discussed below (*11*).

Errors in clear-sky fluxes can also arise from cloud contamination of the so-called clear scenes. Only data from instruments with much better resolution than the ERBE scanner can provide an accurate estimate of this bias error. Lacking such data, we attempted various consistency checks on a sample of the clear-sky fluxes to examine the size of the error. (i) We applied stringent homogeneity criteria in the identification of clear scenes. (ii) We chose scenes for which the eight surrounding scanner pixels were also clear. (iii) We adopted only those scenes for which the σ of the LW radiance was less than 1 percent of the mean LW flux for the nine pixels. The use of these criteria, chosen because of the results presented in (*12*), yielded lower albedos (Fig. 2) and larger LW fluxes than the general results for these scenes (Fig. 1). This response to editing of the data suggests that clouds did contaminate the operational data. However, the bias is only +0.8 percent for albedo and −4 W/m^2 for LW flux. The positive bias in the clear-sky albedo reduces the size of the negative SW cloud forcing. In contrast, the negative bias in the clear-sky LW flux reduces the size of the LW cloud forcing. Because the two forcing terms have opposite signs, the two bias errors partially cancel in the net cloud forcing (Fig. 2). The observed albedos are also consistent with those computed from a detailed theoretical model (Fig. 2) (*10*). The consistency between theory and observations builds confidence in the retrieved clear-sky fluxes. More detailed studies of scene identification errors with several alternative techniques (*7*) also gave results that were similar to those shown in Fig. 2.

LW and SW cloud forcing. The LW cloud forcing (Fig. 3A) reaches peak values over tropical regions and decreases toward the poles. In general, clouds reduce the LW emission to space. This reduction in emission is effectively an increase in the radiation energy absorbed in cloudy regions (compared with the energy in clear-sky regions). Because the reduction in the LW emission is largely a result of the emission from cold cloud tops, optically thick, high clouds reduce the emission more than low clouds. Hence, cloud forcing of 50 to 100 W/m^2 is at a maximum in regions with extensive cirrus cloud decks. Maxima occurred in three regions: (i) the tropical Pacific and Indian oceans surounding Indonesia and the Pacific intertropical convergence zone north of the equator; (ii) the monsoon region in Central Africa and the deep convective regions of the northern third of South America; and (iii) the mid-latitude storm tracks in the Pacific and Atlantic oceans.

The SW cloud forcing (Fig. 3B) shows peaks in the mid-latitudes, unlike the LW forcing. In the tropics, large negative values were observed in the tropical monsoon and deep convective regions (Fig. 3A). These are areas where the LW forcing was equally large; the SW forcing was also large north of 30°N in the Atlantic and Pacific oceans. In these regions, the reduction of absorbed solar radiation as a result of clouds exceeded 100 W/m^2. Cloud systems associated with the mid-latitude storm tracks and extensive stratus decks over the colder oceans were responsible for this large reduction (*13*). Large (negative) values were also observed over the oceans in the mid-latitude Southern Hemisphere. These regions are known as the "roaring 40's" because of the persistence of cyclones. Both SW and LW cloud forcing were negligible over the narrow band of oceanic upwelling regions of the eastern and central Pacific oceans. In summary, cloud forcing patterns, even for observations during 1 month, reflect the major climatic regimes and the organized cloud systems of the planet. Distinguishing between clear and cloud scenes over the bright ice and snow-covered regions is difficult, and therefore the positive SW forcing results over and near the Arctic are less accurate than elsewhere; even the sign of the effect may be uncertain.

In tropical regions, where the clouds significantly affected the LW and SW fluxes, the LW and SW terms nearly cancel each other. The net forcing there (Fig. 4) was within ±10 W/m^2, roughly the estimated uncertainty in our regional estimates of the net cloud-radiative forcing. Between 15°N and 15°S, the zonally averaged forcing was slightly negative and was about 10 to 20 percent of the SW forcing. Earlier workers (*14*) anticipated the competing nature of the two forcing terms. However, their near cancellation is surprising. We do not understand the physical and dynamical constraints that require these cloud systems to organize in such a manner. The only exceptions to the near cancellation of the cloud forcing in the tropics are marine stratocumulus cloud systems. These systems commonly occur off the coast of Chile (in South America) and the coasts of Angola and Namibia in Africa.

Near cancellation of the column-integrated radiative forcing does not imply a negligible role of clouds in the regional climate. Modeling results (*6*) suggest that the negative C_{SW} is due to divergence (cooling) of SW flux at the earth's surface. In contrast, the positive C_{LW} in the tropics is due to convergence (heating) of LW flux in the troposphere. Thus these cloud systems may lead to a significant perturbation of the vertical gradients of radiative heating or cooling patterns (*6, 15*).

Over the mid- to high-latitude oceans, poleward of 30° in both hemispheres, cloud forcing is negative. The negative forcing is particularly large over the Pacific and Atlantic oceans where C is between −50 and −100 W/m^2.

Another anomalous feature (Fig. 4) is the positive cloud forcing regions in the Western Sahara Desert and the Sahel regions of Africa. The positive values over the desert regions arise from the LW cloud forcing (Fig. 3), accompanied by negligible SW forcing. Cloud forcing is also positive over the snow-covered regions of Canada and the Arctic, where both the LW and the SW forcing terms are positive. However, as mentioned earlier, the clear-sky estimates over snow-covered regions are subject to large uncertainty. A better clear-sky discriminator and more extensive seasonal sampling are needed to confirm the forcing estimates over these regions.

Climatic implications. Cloud forcing reduces the absorbed solar radiation by 44.5 W/m^2 and the LW emission to space by 31.3 W/m^2

when averaged over the globe (Tables 2 and 3). Thus, globally, clouds reduce the radiative heating of the planet by 13.2 W/m^2 (Table 3). This conclusion is based on data from just 1 month. Data for July 1985, October 1985, and January 1986 are now being processed. Preliminary analyses of these months confirm the basic finding of this study: clouds have a net cooling affect on the global climate. There are significant month-to-month differences in the net cooling effect. It attained a maximum value of -21.3 W/m^2 in January 1986 (Table 3). The differences in the monthly values are a result of both seasonal and interannual variations in the parameters that govern cloud forcing. The data for the 4 months indicate the likely range of planetary radiative cooling due to clouds during a year.

Studies with GCM's provide some assessment of the climatic significance of this radiative cooling. Several studies have suggested that radiative heating of a mere 4 W/m^2 resulting from a doubling of CO_2 concentrations in the atmosphere would lead to a global warming of 3.5 to 5 K (*4*). The negative cloud-radiative forcing is three to five times as large as the doubled CO_2 forcing. The size of the forcing suggests that the planet would be significantly warmer without the current cloud-radiative forcing.

Cloud forcing has also been inferred from GCM's (*15, 16*). The GCM results are in qualitative agreement with those shown here. For both observations and models $C_{LW} > 0$, $C_{SW} < 0$, and $C < 0$. However, there are significant quantitative differences between the various models (Table 3) (*16*). The next step in identifying deficiencies in model simulations is to compare the regional and seasonal variations in the cloud forcing fields.

Cloud-climate feedback. A change in climate can perturb the cloud forcing, which in turn can feed back into the initial climate change. Thus, observations of long-term changes in cloud forcing can provide insights into the nature of the cloud-climate feedback. Two of the important feedback mechanisms suggested by our data are described below.

In mid- to high-latitude oceanic regions, strong negative forcing over the oceans coincides with regions of stratus and the storm tracks of mid-latitude cyclones. The frequency, as well as the latitudinal extent of these storms, couples to latitudinal temperature gradients (*13*). Large changes in the latitudinal temperature gradients accompany a climate change, such as the last ice age which occurred about 15,000 years ago (*17*). For example, during the glacial maximum, the mid-to-polar Atlantic Ocean was 5 to 10 K cooler than at present, while the subtropical oceans were less than 2 K cooler (*17*). In response to this enhanced temperature gradient and southward migration of the cold waters, the storm track clouds and the stratus decks might have shifted southward. Then, the regions where C was less than -50 W/m^2 would have also shifted southward and amplified the cooling. This mechanism is similar in principle to the ice-albedo feedback (*1, 4*). The effect of a shift from 45°N to 35°N of, for example, the -50 to -75 W/m^2 cloud forcing region is large. Such a shift, if it persists through the year, could induce a hemispherical average radiative cooling of roughly 3 W/m^2. This cooling is larger than the radiative effect of the observed decrease in CO_2 concentration from 300 to 180 ppm that occurred during the glacial maximum 15,000 to 20,000 years ago (*18*).

Tropical convective cloud systems contain a mixture of cumulus, cumulonimbus, and cirrus anvils (*19*). Despite the considerable discussion on the effect of tropical clouds, we still do not know whether the reflective cloud forcing of the cumulus clouds or the heating effect of the cirrus is dominant (*4, 5*). Our data suggest that these effects nearly cancel when integrated over the column. Some GCM's had anticipated this near cancellation of the LW and SW cloud forcing (*6*). However, these clouds can play a substantial role in climate change for two reasons: (i) The height of cloud tops largely governs the LW cloud forcing, but the water and ice content determine the SW forcing. (ii) Surface temperature influences the height but low-level convergence governs the water content. As an example, a warming due to the observed increase in CO_2 and other trace gases could increase the height of these clouds (*5*), which would increase C_{LW}. Because the individual forcing terms are large, a change in either of them would have a similar effect on the net cloud forcing.

In summary, the cloud forcing concept contributes to our understanding of climate and climate change. First, cloud forcing is an important part of the energy flow of the earth-atmosphere system. Second, we can quantitatively estimate cloud forcing from radiation budget measurements by broadband scanners. Third, we must be able to predict changes in cloud forcing if we are to predict the total response of climate to various perturbations. Such perturbations include orbital variations that have been implicated in earlier ice age episodes and changes that are expected from trace gas increases.

Observations of long-term changes in cloud forcing can be used directly to provide confirmation of previously untestable ideas (*5*) and climate model results (*4*) regarding climate change. For example, results from some GCMs suggest that severe drying of the mid-continental regions in North America and Europe could result from a doubling of the CO_2 concentrations (*4, 20*). In the Great Plains region of North America, the summer soil wetness in one model is decreased by 50 percent (*20*, figure 7), which suggests that a positive feedback between clouds and land surface could be a factor in soil drying (*20*). An initial tendency for drying causes decreased cloudiness, which leads to increased solar heating of the soil, thus amplifying tendency toward drying. The positive cloud feedback mechanism implies that the size of the (negative) SW cloud forcing would decrease significantly during a drought event. According to Manabe and Wetherald (*20*) the decrease could be as much as 25 W/m^2 in the Great Plains. The LW forcing should also decrease, but the model results suggest that changes in the SW cloud forcing dominate the feedback. Cloud forcing data could verify this postulated positive cloud feedback. For example, this mechanism would imply that the summertime SW cloud forcing over the Great Plains was anomalously low during the 1988 drought. Comparison of the cloud forcing for this year with the forcing for other years should confirm or refute this suggestion.

REFERENCES AND NOTES

1. R. D. Cess, *J. Atmos. Sci.* **33**, 1831 (1976); J. S. Ellis, thesis, Colorado State University, Fort Collins (1978). These are two of the earlier studies in which an attempt was made to assess the role of clouds from satellite radiation budget measurements. Ellis also estimated cloud-radiative forcing from regional radiation budget data. See S. H. Schneider [*J. Atmos. Sci.* **29**, 1413 (1972)] for a discussion of the cloud-climate feedback.
2. Cess and Ellis (*1*) estimated that the global greenhouse effect due to clouds was between 20 and 40 W/m^2. A hundredfold increase in CO_2 concentration would effectively trap about 25 W/m^2.
3. D. L. Hartmann *et al.*, *Rev. Geophys. Space Phys.* **24**, 439 (1986).
4. J. Hansen *et al.*, *Climate Processes and Climate Sensitivity*, Maurice Ewing Series (American Geophysical Union, Washington, DC, 1984), p. 130; C. A. Wilson and J. F. B. Mitchell, *J. Geophys. Res.* **92**, 13315 (1987); W. M. Washington and G. A. Meehl, *ibid.* **89**, 9475 (1984); R. T. Wetherald and S. Manabe, *J. Atmos. Sci.* **45**, 1397 (1988).
5. R. C. J. Somerville *et al.*, *J. Geophys. Res.* **89**, 9668 (1984); R. J. Charlson, J. E. Lovelock, M. O. Andreae, S. O. Warren, *Nature* **326**, 665 (1987).
6. V. Ramanathan, *J. Geophys. Res.* **92**, 4075 (1987).
7. B. R. Barkstrom, *Bull. Am. Meteorol. Soc.* **65**, 1170 (1984); ERBE science team (B. R. Barkstrom *et al.*), *ibid.* **67**, 818 (1986); R. B. Lee, B. R. Barkstrom, R. D. Cess, *Appl. Opt.* **26**, 3090 (1987).
8. The ERBS is in a midinclined orbit, which precesses through all local hours at the equator in 36 days. The NOAA-9 is in a sun-synchronous orbit with equatorial crossing times at 0230 and 1430 local solar time. This multisatellite configuration significantly reduces the temporal sampling errors in earlier satellite measurements. For example, see E. F. Harrison, P. Minnis, G. G. Gibson, *J. Spacecr. Rockets* **20**, 491 (1983).
9. Satellite radiation budget data are the traditional source for domain average values of F, α, and H [see T. H. Vonder Haar and V. E. Suomi, *Science* **163**, 667 (1969)].

We refer to these domain average values as cloudy-sky values. They are, in principle, a composite of clear and overcast sky values. To compute cloud forcing, we require both these cloudy-sky values and the clear-sky values. From the scanner pixels, we look for hole in the cloud cover. These holes we identify as the clear-sky scenes. Their fluxes give us the clear-sky values in each domain of 2.5° latitude by 2.5° longitude. (Further details of the clear-sky algorithms are given in B. A. Wielicki and R. N. Green, in preparation.)
10. B. P. Briegleb *et al.*, *J. Climatol. Appl. Meteorol.* **25**, 214 (1986).
11. A simple picture of the sampling error suggests that it should vary as $\sigma/\sqrt{N}$, where N is the number of independent samples. Typically, for a region 2.5° by 2.5°, over a period of 1 month, N should be about 10. The main point is that the sampling error should be smaller than the σ (Table 1) by a factor of 2 or more.
12. J. A. Coakley and F. P. Bretherton, *J. Geophys. Res.* **87**, 4917 (1982). This paper shows that the clear-sky LW radiance over the oceans is characterized by very low σ's.
13. E. Palmen and C. W. Newton, *Atmospheric Circulation Systems* (Academic Press, New York, 1969).
14. D. L. Hartmann and D. A. Short, *J. Atmos. Sci.* **37**, 1233 (1980); G. Ohring and P. F. Clapp, *ibid.*, p. **447**.
15. T. D. Charlock and V. Ramanathan, *ibid.* **42**, 1408 (1985); A. Slingo and J. M. Slingo, *Q. J. R. Meteorol. Soc.* **114**, 1027 (1988).
16. R. D. Cess and G. L. Potter, *Tellus* **394**, 460 (1987).
17. H. H. Lamb, *Climatic History and the Future* (Princeton Univ. Press, Princeton, NJ, 1985).
18. J. Jouzel *et al.*, *Nature* **329**, 403 (1987).
19. A. F. Bunker and M. Chaffee, *Tropical Indian Ocean Clouds* (East-West Center Press, Honolulu, HI, 1969).
20. S. Manabe and R. T. Wetherald, *J. Atmos. Sci.* **44**, 1211 (1987).
21. Supported in part by the NASA ERBE Project; NSF grant ATM8700286 (V.R. and E.A.). We thank the ERBE Science Team and the project scientists at NASA Langley Research Center for making this work possible, G. Gibson for the graphics, and two anonymous referees for their comments.

18 July 1988; accepted 28 November 1988